STEM CELLS®

TRANSLATIONAL AND CLINICAL RESEARCH

Extracellular Vesicle-Shuttled mRNA in Mesenchymal Stem Cell Communication

ENRICO RAGNI,[a] FEDERICA BANFI,[a] MARIO BARILANI,[a,b] ALESSANDRO CHERUBINI,[a] VALENTINA PARAZZI,[a] PAOLA LARGHI,[c,d] VINCENZA DOLO,[e] VALENTINA BOLLATI,[f,g] LORENZA LAZZARI[a]

Key Words. Mesenchymal stem cells • Extracellular vesicles • mRNA • IL-10

ABSTRACT

Mesenchymal stem cells (MSC) are multipotent cells able to differentiate into several cell types, hence providing cell reservoirs for therapeutic applications. The absence of detectable MSC homing at injury sites suggests that paracrine functions could, at least in part, be mediated by extracellular vesicles (EVs); EVs are newly identified players that are studied mainly as predictive or diagnostic biomarkers. Together with their clinical interests, EVs have recently come to the fore for their role in cell-to-cell communication. In this context, we investigated gene-based communication mechanisms in EVs generated by bone marrow and umbilical cord blood MSC (BMMSC and CBMSC, respectively). Both MSC types released vesicles with similar physical properties, although CBMSC were able to secrete EVs with faster kinetics. A pattern of preferentially incorporated EV transcripts was detected with respect to random internalization from the cytosol, after a validated normalization procedure was established. In the paradigm where EVs act as bioeffectors educating target cells, we demonstrated that kidney tubular cells lacking *IL-10* expression and exposed to BMMSC-EVs and CBMSC-EVs acquired the *IL-10* mRNA, which was efficiently translated into the corresponding protein. These findings suggest that horizontal mRNA transfer through EVs is a new mechanism in the MSC restoring ability observed in vivo that is here further demonstrated in an in vitro rescue model after acute cisplatin injury of tubular cells. STEM CELLS *2017;35:1093–1105*

SIGNIFICANCE STATEMENT

Mesenchymal stem cells (MSC) since many years are on the edge of innovation aimed at future therapeutic applications. Many pathways explaining MSC potential have been discovered and dissected. Despite such promising results, a clear picture of biological action is missing rendering the choice of the most favorable cell type unattendable. This work demonstrates that secreted vesicles may shuttle therapeutic messenger RNA to recipient cells to educate them in order to reduce inflammation and cell death. Such new evidence adds a new player to the existing knowledge aimed at the definition of MSC potential.

INTRODUCTION

Mesenchymal stem cells (MSC) are multipotent, non-hematopoietic adult stem cells, which can be isolated from almost all tissues and possess in vitro multilineage differentiation into mesodermic, endodermic, and ectodermic lineages [1, 2]. During the last 10 years, these multipotent cells have generated considerable interest owing to their immunomodulatory activity and ability to escape the allogeneic immune response [3]. Such unique properties make MSC an invaluable cell type for the repair of tissue/organ damage, attracting attention as a potential solution for tissue repair and wound healing [4]. Multiple mechanisms identifying how MSC mediate their regenerative and immunomodulatory effects have been proposed, although, to date, several ambiguities and inconsistencies persist [5].

The initially proposed differentiation-based rationale for MSC use has become increasingly untenable. MSC engraftment and subsequent differentiation into appropriate cell types were rare, with <1% of the administered cells surviving for more than 1 week [6–8]. Therefore, the predominantly short-lived paracrine effects of MSC became evident [9–11]. The paracrine effects of MSC were shown to include the release of both soluble factors, and extracellular vesicles (EVs) as parallel mechanisms for cell-to-cell communication [12].

EVs are composed of at least two distinct subtypes: exosomes (40-100 nm in diameter) formed within the endosomal network and

[a]Cell Factory, Unit of Cell Therapy and Cryobiology, Fondazione IRCCS Ca' Granda Ospedale Maggiore Policlinico, Milan, Italy; [b]Department of Industrial Engineering, University of Padova, Padova, Italy; [c]Autoimmunity Program, Istituto Nazionale di Genetica Molecolare "Romeo Ed Enrica Invernizzi", Milan, Italy; [d]Department of Pathophysiology and Transplantation, University of Milan, Milan, Italy; [e]Department of Life, Health and Environmental Sciences, University of L'Aquila, L'Aquila, Italy; [f]EPIGET - Epidemiology, Epigenetics and Toxicology Lab, Department of Clinical Sciences and Community Health, University of Milano, Milan, Italy; [g]Epidemiology Unit, Fondazione IRCCS Ca' Granda Ospedale Maggiore Policlinico, Milan, Italy

Correspondence: Lorenza Lazzari, Ph.D., Cell Factory, Unit of Cell Therapy and Cryobiology, Fondazione IRCCS Ca' Granda Ospedale Maggiore Policlinico, Via F. Sforza 35, Milan 20122, Italy. Telephone: +390255034053; Fax: +390255032796; e-mail: lorenza.lazzari@policlinico.mi.it

Received June 6, 2016; accepted for publication November 27, 2016; first published online in STEM CELLS *EXPRESS* December 21, 2016.

1066-5099/2016/$30.00/0

http://dx.doi.org/10.1002/stem.2557

microvesicles (100-1,000 nm) produced by outward budding of the plasma membrane. Cargo components and loading mechanisms are still a matter of debate, although it has become clear that specific subsets of lipid, protein, and nucleic factors may distinguish both EVs sub-populations and EVs secreted from different cell types [12]. The emerging role for EVs as a shuttle of bioactive molecules, either as mediators to educate the surrounding environment or as screening markers in early-stage diagnosis, is being investigated, particularly by cancer researchers.

In the stem cell field, recent reports have demonstrated beneficial EVs effects in in vitro and animal models of kidney, liver, and lung injury and wound healing (reviewed in Rani et al. [13]), together with a low propensity to trigger innate and adaptive immune responses [14]. Because EVs appear to recapitulate the therapeutic effects of stem cell transplantation, the prevailing hypothesis is that MSC-EVs may exert their effects by transferring biologically active molecules such as proteins, lipids, and various classes of nucleic acids including transcripts encoding therapeutic mediators. Therefore, the goal of our work was to characterize MSC-EV mRNAs and demonstrate a clear proof-of-concept for the efficient transfer of EV mRNAs to target cells and their subsequent translation in those cells as a novel mechanism of cellular communication.

Materials and Methods

Cell Isolation and Growth

MSC from bone marrow aspirate and umbilical cord blood were obtained from healthy donors after informed consent. MSC isolation was performed as described in Ragni et al. [15]. MSC were propagated in alpha MEM supplemented with 20% Fetal Bovine Serum (FBS) (Life Technologies, Carlsbad, CA, https://www.thermofisher.com/). Stem cell identity of isolated bone marrow MSC (BMMSC) and cord blood MSC (CBMSC) was confirmed by immunophenotype profile: cells were negative for the pan-hematopoietic marker CD45 and positive for the MSC cell-surface antigens CD73, CD90, and CD105, officially recommended for their concurrent use to define unambiguously a MSC type [16]. MSC were able to differentiate in vitro into adipocytes, osteocytes and chondrocytes following what reported in Ragni et al. [17] (data not shown). All subsequent studies were carried out in technical triplicate on two independent cell lines named #1 and #2. Experiments were performed at passage 5. Human proximal tubular cells HKC8 were cultured in DMEM/F12 media supplemented with 10% FBS.

EVs Preparation

MSC were grown to 80% confluence and then fresh medium without FBS was added. After 4-8-24 hours, conditioned culture medium was collected and serially centrifuged to remove floating cells and cellular debris (400*g* for 10 minutes and 5,000*g* for 15 minutes for three times) before being ultracentrifuged at 100,000*g* for 1 hour at 4°C with a fixed angle rotor (Fiberlite F37L-8x100) (Thermo Fisher Scientific, San Francisco, CA, https://www.thermofisher.com/). The pellet was suspended in PBS, dissolved in lysis buffer for RNA extraction or RIPA buffer for protein analysis.

Scanning Electron Microscopy

MSC grown on a glass coverslip were first fixed in 2% glutaraldehyde (Electron Microscopy Sciences, Hatfield, PA, https://www.emsdiasum.com/microscopy/) in PBS and then dehydrated through a graded series of ethanol solutions. Samples were critical-point dried and sputter coated with a SCD040 Balzer Sputterer (Balzers Union, Balzers, Liechtenstein, https://www.oerlikon.com/balzers/com/en/). A SEM Philips 505 scanning electron microscope (Philips, Eindhoven, The Netherlands, https://www.fei.com/) was used to examine the samples, using an accelerating voltage of 20 kV.

Transmission Electron Microscopy

According to proper dilutions, the EVs suspended in Phosphate Buffer Saline (PBS) were adsorbed to 300 mesh carbon-coated copper grids (Electron Microscopy Sciences, Hatfield, PA) for 5 minutes in a humidified chamber at room temperature. Vesicles on grids were then fixed in 2% glutaraldehyde in PBS for 10 minutes and then briefly rinsed in milli-Q water. Grids with adhered vesicles were examined with a Philips CM 100 transmission electron microscope TEM at 80kV, after negative staining with 2% phosphotungstic acid, brought to pH 7.0 with NaOH. Images were captured by a Kodak digital camera.

Measurement of Particle Number and Size Distribution by Nanoparticle Tracking Analysis

Nanoparticle tracking analysis (NTA) was carried out using the Nanosight system (NanoSight, Wiltshire, UK, www.malvern.com/) on EVs suspended in PBS that were further diluted 50-fold for analysis. NTA related the rate of Brownian motion to particle size. Vesicles were visualized by light scattering using a conventional optical microscope aligned perpendicularly to the beam axis. After a video was taken, NTA software tracked between frames the Brownian motion of individual vesicles and calculated total concentration and their size through application of Stokes-Einstein equation.

PKH26-Labeled EVs Transfer

EVs suspended in Diluent C were mixed with PKH26 (Sigma-Aldrich, St. Louis, MO, https://www.sigmaaldrich.com/) and incubated for 20 minutes at RT in the dark. Labeling reaction was stopped by adding an equal volume of 1% BSA. EVs were ultracentrifuged at 100,000*g* for 1 hour, washed with PBS, ultracentrifuged again at 100,000*g* for 1 hour and finally suspended in PBS. Labeled vesicles were incubated with HKC8 cultured in a 20,000/1 (EVs/cell) ratio. PBS that received the same treatment as above was used as a control. Cells were observed after 24 hours under a Leica SP5 confocal microscope (Leica Microsystems, Wetzlar, Germany, www.leicamicrosystems.com/) or by flow cytometry with a FACSCanto II instrument (Becton Dickinson, San Diego, CA, www.bd.com/) by measuring the fluorescence of PKH26 detected at 567 nm.

Determination of the Number of EVs Incorporated by Kidney Tubular Cells

PKH26-labeled EVs were administrated to HKC8 cells with a 20,000/1 EVs/cell ratio. After 24 hours, cells were washed, detached, and suspended in PBS to a concentration of 1,000,000 cell/ml. 0.1 ml was analyzed by ELISA in a 96-well plate with a 530 nm filter for PKH26 excitation and a 570 nm

filter for PKH26 emission. Cells treated with unlabeled EVs were used as negative CTRL and to subtract fluorescence background. In a separate well, $2.5exp^9$ PKH26-labeled vesicles suspended in 0.1 ml PBS were also scored for fluorescence. Signal intensity of EVs-treated cells after background subtraction was compared to labeled EVs fluorescence to determine the number of incorporated EVs.

qRT-PCR Analysis

RNA was isolated using RNeasy Micro kit (Qiagen, Hilden, Germany, www.qiagen.com/). Quantitative PCR was carried out using "SsoFast EvaGreen Supermix" (Bio-Rad Laboratories, Hercules, CA, www.bio-rad.com/). Gene specific primers (Neuroprotection: *NGF, BDNF, GDNF, NTF3, CDNF, CNTF, MANF;* Proliferation: *FGF2, FGF7, ANGPT1, ANGPT2, CTGF, HGF, VEGF;* Immunomodulation: *IL-4, IL-6, IL-10, IL1RN, TGF-β1, TNFα;* Stemness: *ALCAM, BMP2, BMP7, KDR, PDGFRB, THY1, BGLAP, COL1A1, ICAM1;* Housekeeping: *GAPDH*) were used. Triplicates of all reactions were analyzed. All replicates should be within 0.5 Ct of each other for further processing. To confirm product specificity, a melting curve analysis and an agarose gel electrophoresis for the less abundant transcripts were performed after each amplification. Relative gene expression was normalized in EVs using a combined method relying on *GAPDH*, mean Ct value and cDNA input (see Results). For MSC and to compare MSC and EVs, *GAPDH* was used. For statistical analysis and expression data generation, the Bio-Rad CFX Manager software was used. Primer sequences will be provided upon request.

RT-PCR Analysis of 3′UTR and Full Length IL-10

RNA was isolated as previously described. cDNA was prepared using SuperScript IV VILO (Thermo Fisher Scientific) following manufacturer's instructions. RT-PCR was carried out using GoTaq Green Master Mix (Promega, Madison, WI). To design 3'UTR specific primers, online tool http://utrdb.ba.itb.cnr.it/ search was first used to identify 3'UTR sequences of *IL-6*, *MANF*, *BGLAP*, and *IL-4* transcripts. Then, Forward and Reverse primers were designed in the first or last 50 bp of the 3'UTR sequences, respectively. Expected RT-PCR amplificates were: *IL-6* 392 bp out of 429 bp, *MANF* 296 bp out of 308 bp, *BGLAP* 157 bp out of 158 bp, *IL-4* 79 bp out of 89 bp. For full length *IL-10* transcript, Forward and Reverse primers were designed in the first 50 bp of the 5′UTR or last 50 bp of 3′UTR of *IL-10* mRNA sequence deposited in NCBI Nucleotide database (NM_000572.2, http://www.ncbi.nlm.nih.gov/nucleotide). Expected amplicon was 1,589 bp out of 1,629 bp. Primer sequences will be provided upon request.

Pathway Analysis

After 3′UTR identification, miRNA binding sites within 3′UTR regions of EVs-accumulated mRNA were identified using miRANDA algorithm (http://www.microrna.org/microrna/home.do), with a mirSVR scores < -1.0 to exclude weak hits. Verified mRNA targets of selected miRNAs were identified using miRWalk database (http://www.umm.uni-heidelberg.de/apps/zmf/mirwalk/index.html) (Dweep et al., 2011). Final target lists were then uploaded to GeneCodis tool (http://genecodis.cnb.csic.es/) to find statistically enriched biological processes with respect to the entries of the whole human genome.

Flow Cytometry

To detect carboxyfluorescein succinimidyl ester (CFSE) positive EVs, vesicles were first 1:50 diluted in PBS and then incubated for 30 minutes at RT with 5 μl of CFSE cell-permeable precursor carboxyfluorescein diacetate succinimidyl ester (CFDA-SE). Unlabeled samples were incubated with 5 μl PBS. Finally, stained and unstained EVs were analyzed on a FACSCanto II (BD).

To detect viable cells after 24 hours FBS depletion, MSC were detached with trypsin, washed with PBS and, after suspension, 1/20 volume 7-AAD (7-Aminoactinomycin D) was added 10 minutes incubation at RT. Labeled cells were immediately analyzed on a FACSCanto II (BD). At least 30,000 events were acquired.

Immunostaining

Immunofluorescence experiments were performed on HKC8 cells grown on fibronectin-coated coverslips using standard procedures. Briefly, 24 hours after cell seeding, EVs were delivered into two consecutive administrations (EVs/cell ratio 20,000/1), with a gap of 24 hours between them. Forty hours after first EVs administration, cell secretion was blocked by administration of Brefeldin A (final concentration 10 μg/ml); after 8 hours, Brefeldin A was removed and cells fixed in 4% PFA. Cell permeabilization was performed with 1% saponin for 15 minutes at RT, then a blocking solution of 3% BSA was added for 30 minutes at RT and finally the primary antibody was added in blocking solution at a final concentration of 5 μg/ml (mouse anti-human IL-10, Santa Cruz Biotechnology, Santa Cruz, CA, https://www.scbt.com/) and incubated overnight at 4°C. Goat anti-mouse PE-conjugated antibody was used as secondary antibody, incubating cells for 1 hour at RT. Cell nuclei were stained with DAPI. Images were acquired using a Leica TCS SP5 confocal microscope with HCX PL APO 63x/1.25 objective (Leica). No primary antibody stained and no EVs incubated cells were used to set up experimental conditions and antibody dilutions.

Western Blot

Purified EVs or HKC8 collected 72 hours after EVs administration and 8 hours after Brefeldin A block were suspended in RIPA buffer supplemented with protease and phosphatase inhibitors and denatured in Laemmli Sample Buffer (Bio-Rad Laboratories) at 60°C for 15 minutes. Ten microgram of EVs proteins or 50 μg of cell extracts were separated by SDS-PAGE, transferred onto nitrocellulose membranes and incubated 1 hour at RT with blocking solution (5% BSA in TBS, 0.1% Tween-20) (Sigma-Aldrich). Membranes were incubated overnight at 4°C with the following primary antibodies: (a) mouse anti-human IL-10 (Santa Cruz Biotechnology cat. n° sc-8438, 1:200 dilution in 5% BSA in PBS, 0.1% Tween-20), (b) mouse anti-human CD81 (BD cat. n° 551112, 1:200 dilution in 5% BSA in PBS, 0.1% Tween-20), (c) mouse anti-human CD63 (Santa Cruz Biotechnology cat. n° sc-5275, 1:100 in 5% BSA in PBS, 0.1% Tween-20), (d) mouse anti-human CD90 (Abcam, Cambridge, UK, www.abcam.com/, cat. n° ab133350, 1:100 in 5% BSA in PBS, 0.1% Tween-20), (e) mouse anti-human CD105 (Dako, Glostrup, Denmark, www.agilent.com/en/dako-products, cat. n° M3527, 1:200 in 5% BSA in PBS, 0.1% Tween-20), (f) mouse anti-GAPDH (Millipore cat. n° CS204254, 1:10,000 in 5% BSA in PBS, 0.1% Tween-20). Proteins of interest were detected with HRP-conjugated sheep anti-mouse IgG antibody (1:3,000, Bio-Rad Laboratories) and visualized with the

Amersham ECL Western Blotting Analysis System (GE Healthcare, Amersham, UK, www.gelifesciences.com/).

MTT Assay

1.25exp[4] HKC8 cells were seeded into 96-well plates and, after 24 hours, treated for 6 hours with 10 μM cisplatin. After drug removal, cells were washed twice and 100 μl phenol red-free medium added and this time point was set as 0. At time 0, 24, and 48 hours 20,000 EVs/cell were added. One and 10 ng/ml human recombinant IL-10 (BioLegend, San Diego, CA, www.biolegend.com/) conditions were also used after injury as positive control to score a possible IL-10 protective effect. These concentrations were selected following what reported in published in vivo and in vitro models for IL-10 dependent cisplatin-induced acute injury recovery [18, 19]. At time 0, 24, 48, and 72 hours MTT assay was performed. Briefly, 25 μl of a 3 mg/ml Thiazolyl Blue Tetrazolium Bromide (Sigma-Aldrich) were added to each well and the colorimetric reaction was allowed to proceed for 4 hours at 37°C. Then, 25 μl of 40% SDS were added and the plate incubated overnight at 37°C in the dark. The next day, viable cells with MTT dye uptake were determined by measuring the optical density at 570 nm after background subtraction scored at 650 nm. Values shown are the mean of at least six measurements.

Statistical Analysis

Comparison of variances for the expression of distinct genes was used to analyze the significance of differences using one-way analysis of variance (ANOVA) (GraphPad Prism Software version 6, San Diego, CA, https://www.graphpad.com/). A p value $< .05$ was considered statistically significant.

Results

Characterization of MSC-Derived EVs

Electron microscopy on MSC showed structures resembling EVs protruding from the cell surface (Fig. 1A). Interestingly, EV secretion was located in the peripheral protrusions and concentrated at the edges of the plasma membrane for both MSC types. Then, we followed the capacity of the different MSC to secrete EVs by NTA at 4, 8, and 24 hours after FBS removal (to remove vesicles present in serum). In all MSC, the number of secreted vesicles increased as a function of time with a significant gain at 24 hours ($p < .05$, $N = 5$; Fig. 1B). Because no cell toxicity was observed in FBS starved BMMSC and CBMSC ($\leq$ 10% 7AAD+ cells observed at 0, 4, 8, and 24 hour time points), we chose the 24 hours FBS starvation time point for EVs harvesting.

Using NTA we determined that the EVs of CBMSC and BMMSC ranged in size from 40-50 nm to 600-700 nm, indicating the presence of both exosomes and microvesicles. The mean values for the size of CBMSC-EVs and BMMSC-EVs laid between 230 and 275 nm and did not differ significantly ($p > .05$, $N = 10$; Fig. 1C). Interestingly, the observed particle size suggests the absence of apoptotic bodies, which usually fall into the size range of 1-5 μm. We then used NTA quantification to determine the number of EVs secreted per MSC line as function of the number of seeded cells (Fig. 1C). Notably, the CBMSC samples secreted 1.5-2 times more vesicles than BMMSC ($p < .05$, $N = 10$). The CBMSC #2 sample produced the most EVs/cell within a 24 hours period (5,000 secreted EVs/cell; Fig. 1C). Similar results were obtained after monitoring vesicles released by other independent BMMSC ($N = 4$) and CBMSC ($N = 4$) cell lines (CB/BM EVs ratio of 1.6, $p < .01$, $N = 12$), suggesting no major variability between donors.

To confirm the integrity of analyzed EVs, CFDA-SE staining was performed directly on EV-containing supernatants. Flow cytometry analysis showed that >90% of the particles were positive for staining, indicating that vesicles are intact and contain cytoplasmic esterase reacting with CFDA-SE (Fig. 1D). Purification by ultracentrifugation at 100,000*g* yielded a similar percentage of positive EVs, confirming that the centrifugation step of the isolation protocol does not damage EVs (data not shown). Western blot analysis of BMMSC- and CBMSC-EVs confirmed the expression of both exosome (CD63 and CD81) and MSC (CD90 and CD105) specific markers (Fig. 1E). Finally, transmission electron microscopy images showed an expected morphology consistent with pure EV preparations (Fig. 1F).

Molecular Analysis of MSC-EVs

It has been reported previously that MSC-EVs contain mRNAs [15, 20–23]. While these studies identified some of the encapsulated transcripts, they did not assess their relative expression levels or the ratios between different EV isolates. As detailed in the Materials and Methods, 30 mRNAs characteristic of mesenchymal cells (functions involved in neuroprotection, control of proliferation, and immunomodulation; see Materials and Methods for more details) were quantified in parallel by qRT-PCR. We were able to amplify ($C_t < 40$) 18 transcripts from the EVs of BMMSC #1 and CBMSC #1, and 19 transcripts from the EVs of BMMSC #2 and CBMSC #2. To confirm the specificity of the assay, melting curve tests and agarose gel electrophoresis of amplified DNA were performed comparing EVs and cell extracts (*ALCAM*, *NGF*, *TGFB1*, and *VEGFA*) (Fig. 2A). Interestingly, 11 candidates were always undetectable (*GDNF*, *NTF3*, *CDNF*, *ANGPT1*, *ANGPT2*, *IL-1RN*, *TNF*, *BMP2*, *PDGFRB*, *BMP7*, and *ICAM1*). *HGF* gave positive amplification from EVs from samples BMMSC #2 and CBMSC #2 (both with C_t values > 35). *FGF7*, *COL1A1*, *CNTF*, *CTGF*, and *IL-6* transcripts had the highest expression levels in the MSC-EVs (Supporting Information Table 1).

To obtain reliable EV molecular signatures, we had to decide on a method for normalization. To date, no universal reference mRNA has been identified to compare transcript levels in EVs isolated from independent cell lines. Recently, *GAPDH* mRNA has been proposed as a housekeeping transcript for MSC-EVs [24]. To increase reliability of our analysis, we decided to combine three different and independent normalization approaches. First, we measured *GAPDH* mRNA levels in parallel with the target transcripts. Second, we employed a global mean normalization procedure based on the positively amplified mRNAs. This method has a higher accuracy than the multiple reference gene normalization method when no reliable data about housekeepers are available; however, this method is restricted by the number of detected transcripts [25, 26]. Finally, we also normalized expression to EV volumes, calculated as EV number × EV mean size, assuming that identical EV volumes contain comparable nucleic acid levels. Each normalization procedure generated expression ratios used to calculate a ΔC_t value with respect to BMMSC #1-EVs. Notably, the values obtained from the

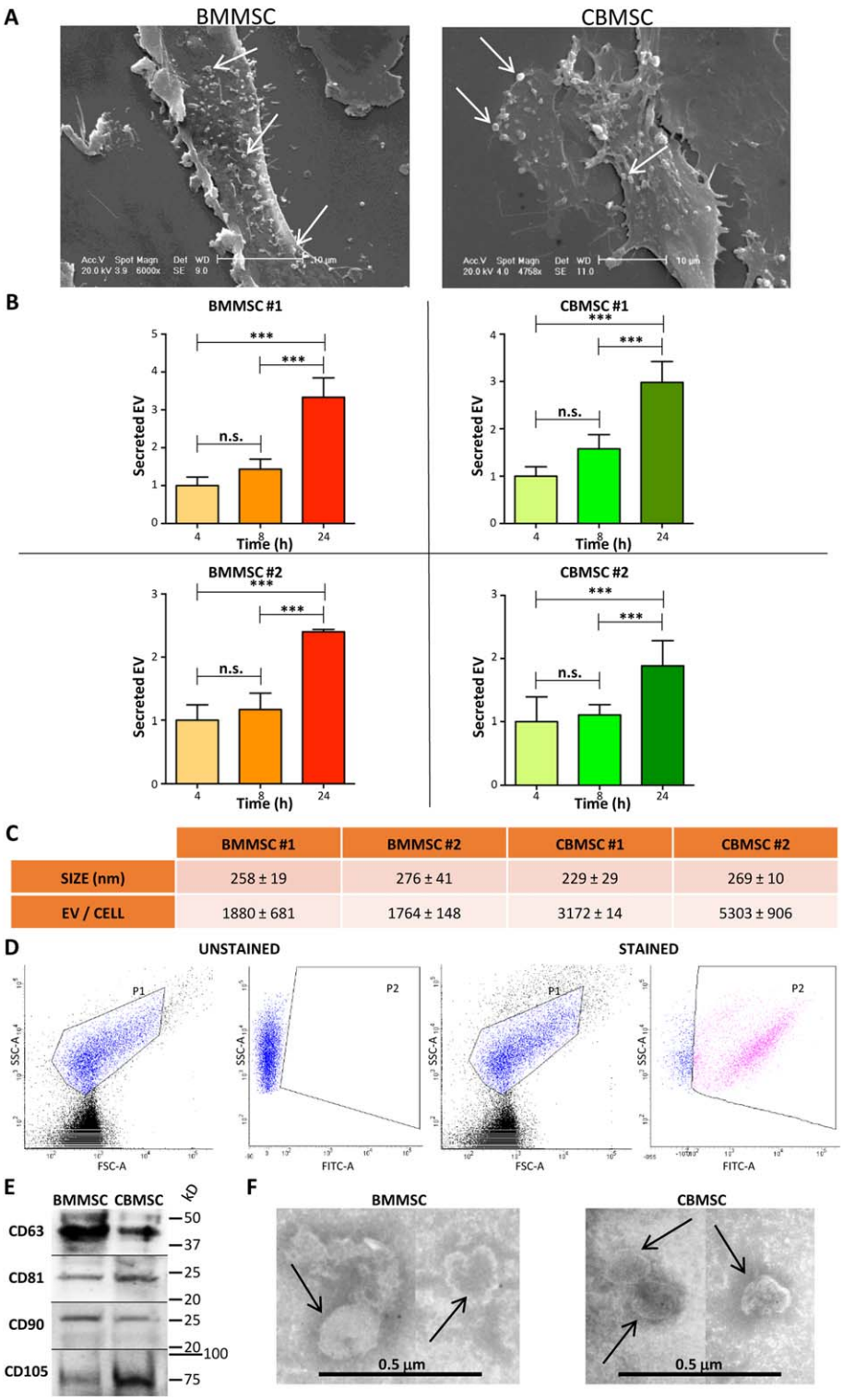

	BMMSC #1	BMMSC #2	CBMSC #1	CBMSC #2
SIZE (nm)	258 ± 19	276 ± 41	229 ± 29	269 ± 10
EV / CELL	1880 ± 681	1764 ± 148	3172 ± 14	5303 ± 906

Figure 1. Kinetics and physical properties of MSC-EVs. **(A)**: Scanning Electron Microscopy of BMMSC and CBMSC showing EVs shedding from cell protrusions. Arrows point out representative examples of vesicles dismissed from the cell surface. **(B)**: EVs secretion kinetics normalized on values at 4 hours set as 1 ($n = 5$ per cell population, errors as SD). Significant differences between groups are noted as *** (p value $< .001$). **(C)**: EVs mean size obtained from Nanosight analysis ($n = 10$ per cell population, errors as SD) together with quantification of EVs secreted per seeded cell at 24 hours after medium change ($n = 10$ per cell population, errors as SD). **(D)**: CFSE staining of a representative EVs sample showing high integrity of isolated vesicles. P1 = total EV; P2 = carboxyfluorescein succinimidyl ester (CFSE) positive EVs. **(E)**: Western Blot analysis of exosome (CD63 and CD81) and MSC (CD90 and CD105) surface markers in purified EVs from BM- and CB-MSC supernatants. **(F)**: Transmission electron microscopy performed on isolated vesicles to visualize their ultrastructural morphology. EVs are indicated with black arrows. Abbreviations: BMMSC, bone marrow mesenchymal stem cell; CBMSC, cord blood mesenchymal stem cell; EVs, extracellular vesicles.

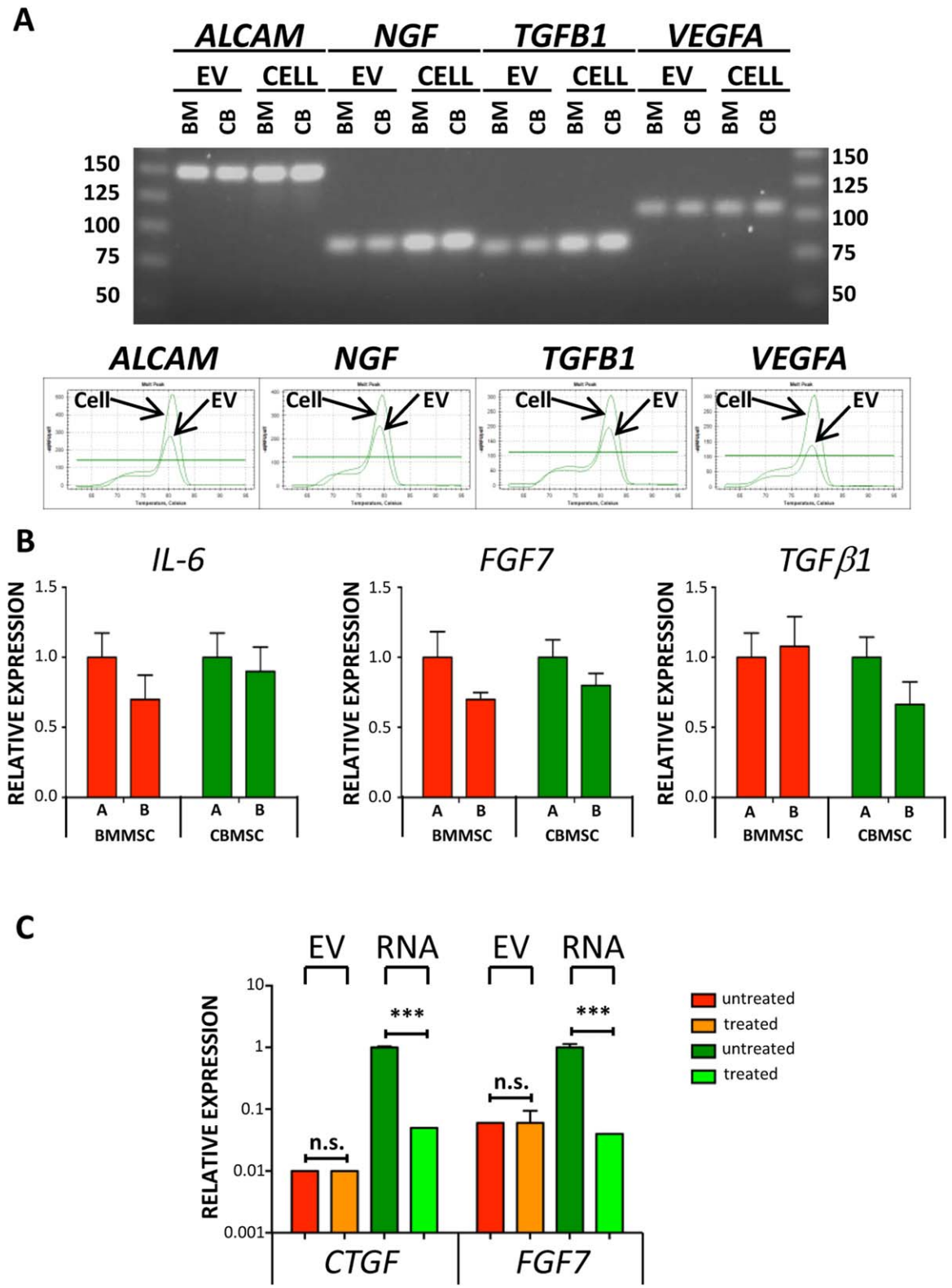

Figure 2. Validation of EV-embedded mRNA transcriptional analysis. **(A)**: Validation of qRT-PCR specificity for low abundant transcripts *ALCAM* (expected 148 bp), *NGF* (85 bp), *TGFB1* (81 bp), and *VEGFA* (105 bp). Agarose gel electrophoresis and representative melting curve tests for BMMSC cell and EVs amplicons are shown. **(B)**: Comparison of *IL-6*, *FGF7*, and *TGFB1* abundance in BMMSC and CBMSC EVs between multiple transcripts analysis (**A**) and individual qRT-PCR (**B**) ($n = 3$ per cell population, errors as SEM). Expression in A was set as 1. **(C)**: *CTGF* and *FGF7* mRNA detection in MSC-EVs analysis after Proteinase K and RNAse A treatment (treated) ($n = 3$ per cell population, errors as SEM). Cell RNA was used as control for positive enzymes digestion, as showed by significant (***, p value $< .001$) reduction in Real-Time PCR amplification. Expression of untreated cell RNA was set as 1. Abberivations: BMMSC, bone marrow mesenchymal stem cell; CBMSC, cord blood mesenchymal stem cell; EVs, extracellular vesicles.

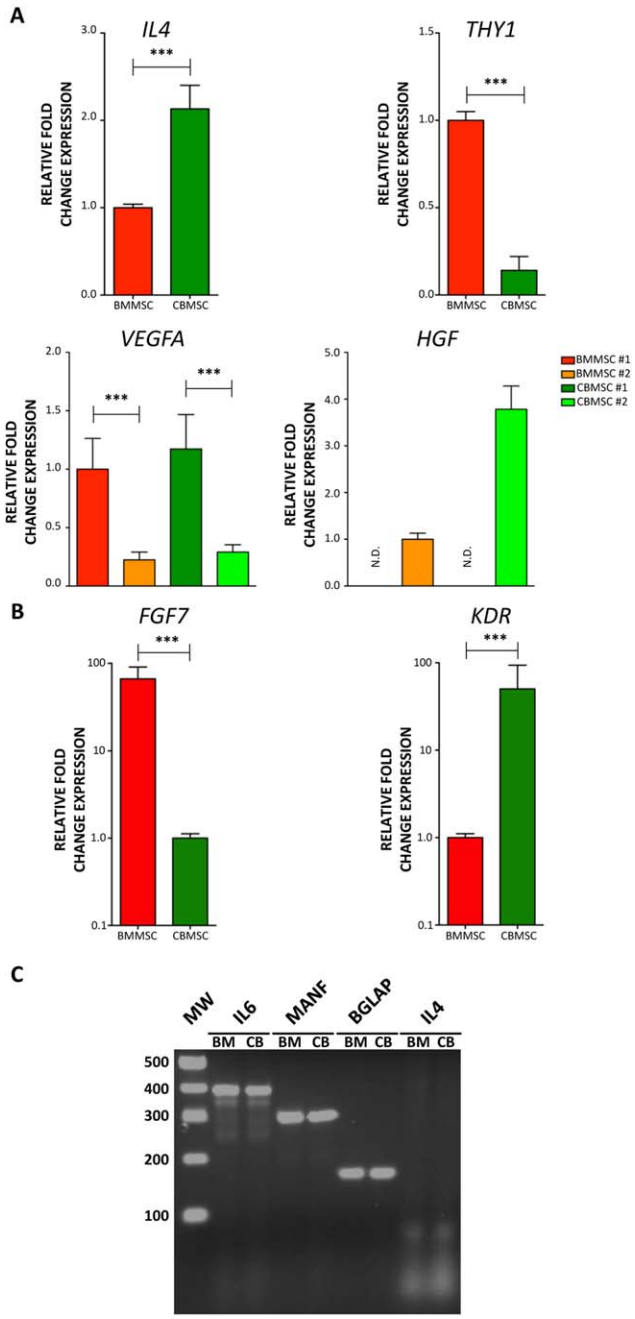

Figure 3. Molecular differences in mesenchymal stem cell (MSC) and secreted extracellular vesicles (EVs). **(A)**: EV-embedded transcripts (*IL-4* and *THY1*) differentially incorporated in CBMSC versus BMMSC (BMMSC set as 1; $n = 6$, errors as SD; ***, p value $< .001$). *VEGFA* and *HGF* showed alternative expression in a cell line dependent fashion (BMMSC #1 set as 1 for *VEGFA* and BMMSC #2 set as 1 for *HGF*, $n = 3$, errors as SD; ***, p value $< .001$). **(B)**: *FGF7* and *KDR* resulted to have significant differential expression in MSC cell extracts (CBMSC set as 1 for *FGF7* and BMMSC set as 1 for *KDR*; $n = 6$, errors as SD; ***, p value $< .001$). **(C)**: Agarose gel electrophoresis analysis of RT-PCR amplification for detection of complete 3′UTR in *IL-6* (expected 392 bp), *MANF* (296 bp), *BGLAP* (157 bp), and *IL-4* (79 bp) EV-embedded transcripts. Abberivations: BMMSC, bone marrow mesenchymal stem cell; CBMSC, cord blood mesenchymal stem cell.

independent methods were similar and therefore averaged for a final normalization value to analyze the qRT-PCR data of the four MSC-EVs under analysis (BMMSC #1-EVs: 1.00; BMMSC #2-EVs: 1.06 ± 0.25; CBMSC #1-EVs: 0.87 ± 0.17; CBMSC #2-EVs: 2.10 ± 0.26).

To exclude potential erroneous mRNA expression detection due to low cDNA input or technical issues, we performed random individual qRT-PCRs on a few selected genes (*IL-6*, *FGF7*, and *TGFB1*) to increase the amount of available template. Notably, results were consistent with those obtained in the initial screening (within twofold modulation) (Fig. 2B). Finally, to confirm that the target mRNAs are present within the vesicles and not just bound to the external membrane surface, isolated EVs were treated with proteinase K and RNAse A. No decrease in the amount of *CTGF* and *FGF7* transcripts was observed, confirming that isolated EVs are intact with mRNA engulfed in the lumen (Fig. 2C).

MSC-EV mRNA Cargo Comparison

The four EV molecular signatures were then compared in order to identify mRNAs that vary significantly in expression between EVs from BMMSC and CBMSC (fold change >2 with $p < .05$). After normalization, no major differences were observed, with few exceptions. CBMSC-EV *IL-4* expression was $>$ 2-fold higher, and *THY1* expression was reduced compared to expression levels in BMMSC-EVs (Fig. 3A). Interestingly, *VEGFA* and *HGF* resulted to have opposite trend, with vascular endothelial growth factor significantly more abundant (two- to fourfold higher) in EVs from BMMSC #1 and CBMSC #1 compared to EVs from BMMSC #2 and CBMSC #2, and hepatic growth factor absent in EVs from BMMSC #1 and CBMSC #1 while it was readily detectable in EVs from BMMSC #2 and CBMSC #2 (Fig. 3A).

The molecular signatures observed for EV types was also found in the corresponding cell extracts, with a few exceptions (Fig. 3B): *FGF7* expression levels were higher in BMMSC (50–100-fold), whereas *KDR* expression levels were more abundant in CBMSC. Therefore, we observed a strong correlation in specific mRNA levels between donor cells and the EVs derived from them, indicating a consistent transcript distribution within these distinct cellular compartments.

The next step was to assess whether some mRNAs were preferentially loaded into EVs with respect to random incorporation from the cytoplasm. Because of its reliability in the previous EV qRT-PCR experiments, *GAPDH* expression was used as a normalization factor. A $>$ 4-fold enrichment or exclusion was chosen as the threshold for analyses. Seven mRNAs were clearly and consistently accumulated in EVs (Table 1). *IL-4* and *IL-10* showed the highest incorporation ratios followed by *BGLAP*, *CNTF*, and *FZD9*. Notably *FGF7* always resulted between the two most detected transcript despite its low expression in CBMSC cell extracts. In contrast, despite their elevated expression in the cytoplasm, *TGFB1* and *ALCAM* resulted under expressed in all four EVs. Finally, of the mRNAs that were not detected in the qRT-PCR assays in EVs, we could not find candidates with high cellular expression, suggesting that their absence of detection was due mainly to low cytoplasm abundance rather than selective exclusion. Altogether, these results suggest preferential loading of some mRNAs into EVs.

3′UTR Analysis of Preferentially Accumulated mRNAs

A recent report suggested that the presence of a core 3′UTR "CTGCC" region (or variations CTGC, CTCCC, CGCCC, TGCC)

Table 1. Differentially enriched mRNA in MSC-EV

BMMSC #1		BMMSC #2		CBMSC #1		CBMSC #2	
GENE	EV/CELL	GENE	EV/CELL	GENE	EV/CELL	GENE	EV/CELL
IL-10	6,472.02	***IL-10***	3,769.09	***IL-4***	9,026.81	***IL-10***	11,425.74
IL-4	2,610.30	***KDR***	3,104.19	***IL-10***	6,517.03	***IL-4***	10,226.32
KDR	1,964.57	***IL-4***	792.35	***BGLAP***	955.43	***FGF7***	744.43
BGLAP	352.14	***BGLAP***	162.02	***FGF7***	245.57	***BGLAP***	680.29
CNTF	125.37	***CNTF***	78.25	***CNTF***	123.64	***KDR***	188.71
FZD9	31.12	***FZD9***	64.89	***FZD9***	119.43	***CNTF***	139.10
FGF7	14.93	***FGF7***	5.43	***KDR***	36.25	***FZD9***	64.89
IL-6	8.82	***NGF***	4.17	***BDNF***	4.28	***BDNF***	5.82
NGF	2.99	***BDNF***	1.77	***FGF2***	1.68	***NGF***	4.17
BDNF	2.62	***IL-6***	1.59	***NGF***	1.38	***FGF2***	2.45
FGF2	1.57	***FGF2***	1.19	***MANF***	0.56	***IL-6***	1.16
MANF	0.81	***THY1***	0.44	***VEGFA***	0.41	***THY1***	0.38
THY1	0.42	***MANF***	0.40	***IL-6***	0.24	***MANF***	0.31
VEGFA	0.37	***CTGF***	0.24	***CTGF***	0.12	***COL1A1***	0.13
COL1A1	0.31	***COL1A1***	0.12	***COL1A1***	0.12	***CTGF***	0.08
CTGF	0.26	***ALCAM***	0.07	***TGFB1***	0.08	***VEGFA***	0.07
TGFB1	0.15	***VEGFA***	0.03	***THY1***	0.08	***TGFB1***	0.03

The amount ratios for indicated gene transcripts in EVs versus cell extracts (EVs/CELL) are shown. The dashed line separates the seven transcripts that are consistently and preferentially accumulated in EVs for all four cell lines used in the study. Values higher than 2 indicate transcripts present in EVs with at least a double amount of what expected from a random internalization from the cytoplasm, whereas values lower than 0.5 indicate messengers excluded in secreted vesicles.

Abberivations: BMMSC, bone marrow mesenchymal stem cell; CBMSC, cord blood mesenchymal stem cell; EVs, extracellular vesicles.

within the wider consensus sequence (CCCCTGCCTGGACC) and/or a miR-1289 binding site may enhance targeting of mRNAs into EVs [27]. After confirmation of full length 3′UTRs (Fig. 3C) in EVs-embedded transcripts as assessed for randomly selected candidates (*IL-6*, *MANF*, *BGLAP*, and *IL-4*), multiple alignment (http://www.ebi.ac.uk/Tools/msa/muscle/) showed the presence of a conserved "core" region in the *KDR*, *CNTF*, *BGLAP*, and *FZD9*, with *FGF7* transcripts harboring the variation *CTGC*. Notably, the CTGCC region was found four times in the 3′UTR of *COL1A1*, the most abundant mRNA in all of the MSC-EVs. On the contrary, the miR-1289 sequence was not found in any of the 3′UTRs tested.

To further identify other potential elements involved in mRNA enrichment, we searched miRNA binding sites within the 3′UTR regions of accumulated mRNAs using the miRANDA algorithm (http://www.microrna.org/microrna/home.do), using a threshold mirSVR score < -1.0 to exclude weak hits. A total of 73 unique sites were identified: 34 miRNA sequences were identified for *FGF7*, 19 for *IL-10*, 19 for *KDR,* 5 for *CNTF*, 3 for *IL-4*, and 2 for *BGLAP* for a total of 73 unique sites. A deeper analysis showed the absence of conserved miRNA binding patterns, with only nine miRNA sites shared by two 3′UTR. Finally, Batagov and colleagues proposed specific sequence motifs (ACCAGCCU, CAGUGAGC, and UAAUCCCA) that may potentially function as *cis*-acting elements targeting RNAs to EVs in glioblastoma cells [28]. None of the five most enriched EV mRNAs contained these elements. Therefore, preferential mRNA loading into EVs may rely on cell type, still unidentified specific motifs, or selectively engulfed mRNA binding proteins able to discriminate between different transcripts, as suggested by Waris et al. [29].

Moreover, it was shown recently that multiple sites for regulatory miRNA binding in 3′UTRs may compete with recipient cell RNAs for binding of miRNA or RNA-binding proteins so as to regulate their stability and translation in recipient cells [30]. Accordingly, we performed a literature-validated gene target identification for the pool of 73 previously identified miRNA using miRWalk, a database of experimentally validated miRNA-gene interactions [31]. The 73 submitted micro-RNAs generated a list of 2,294 potentially regulated targets. Then, we ran these results through the GeneCodis program (http://genecodis.cnb.csic.es/) to find statistically enriched biological processes. We focused our attention on the top five ranked biological processes which were primarily RNA generation and stability GO:0006355 (DNA-dependent regulation of transcription, *p* value 8.57801e-48), GO:0010467 (gene expression, 3.79091e-44), GO:0016070 (RNA metabolic process, 2.57193e-39), GO:0016071 (mRNA metabolic process, 9.8859e-35) and GO:0006915 (apoptotic process, 4.91476e-34) with the majority of apoptosis-related genes being anti-apoptotic (GO:0006916, anti-apoptosis 1.42074e-17). Notably, out of the first 15 categories, 8 were related to various aspects of RNA processing. These results suggest that the inclusion of mRNAs with specific 3′UTR motifs into EVs may have significant effects on the regulation of gene expression in target cells.

mRNA Translation in Recipient Cells

Beside the "miRNA sponge" activity of the 3′UTR, another paradigm of vesicle intercellular communication is that EVs may shuttle functional mRNAs that can be internalized and translated. Therefore, immunomodulatory transcripts embedded in MSC-EVs, together with secreted factors, could be important players for the paracrine properties of MSC. To test this hypothesis, we used a human-derived renal proximal tubular cell line (HKC-8) as the target cell; in a previous publication we assessed the in vivo anti-inflammatory action of BMMSC and CBMSC supernatants in mice with Acute Kidney Injury (AKI) induced by cisplatin treatment [32].

EVs were labeled with the membrane-dye PKH26 without altering membrane integrity (data not shown). After a 24 hours co-culture, the labeled EVs were engulfed by 100% of HKC8 cells, as shown by FACS analysis and confocal microscopy (Fig. 4A, 4B). In our experimental settings, both EVs were incorporated

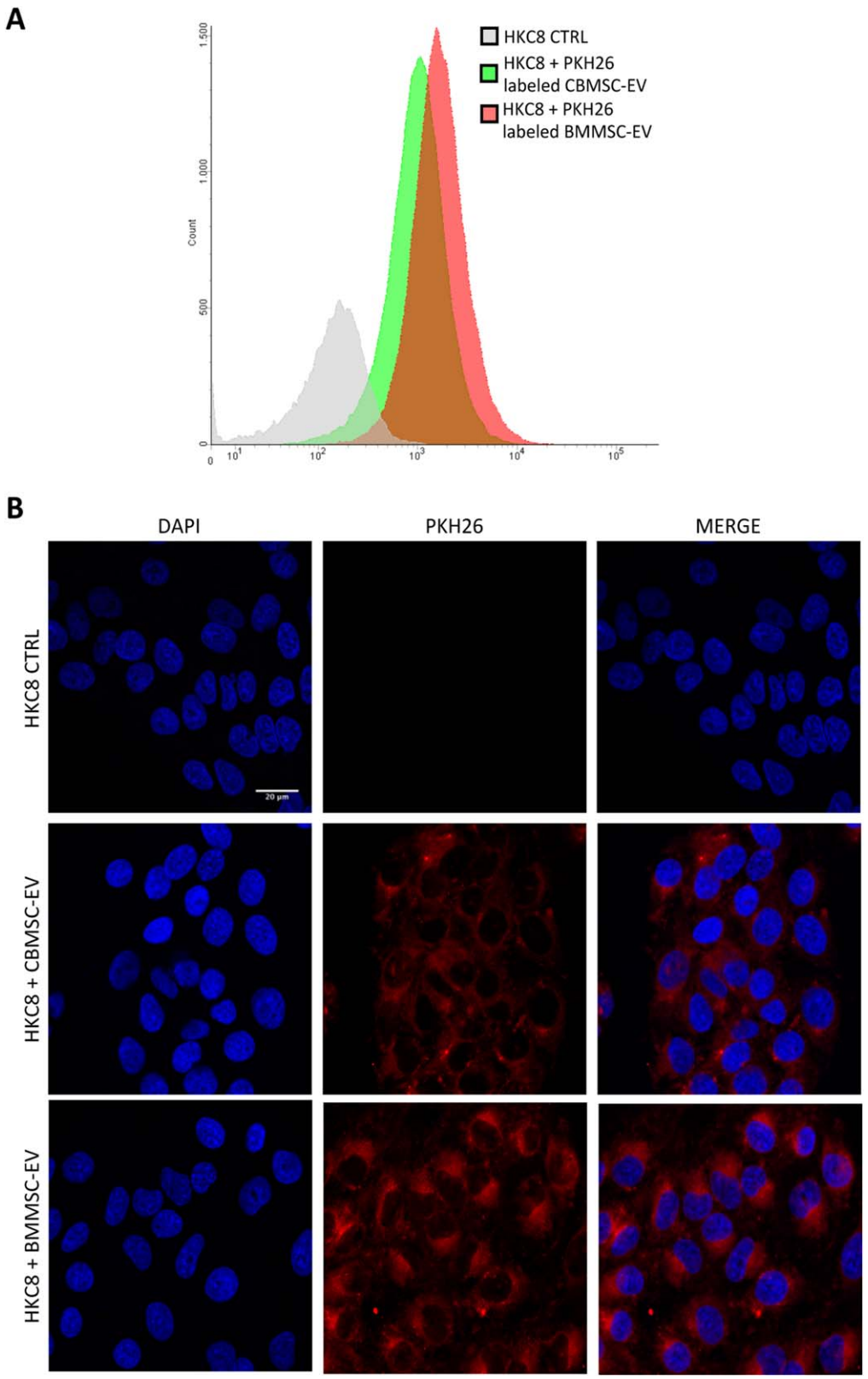

Figure 4. PKH26 EVs labeling and HKC8 incorporation. **(A)**: FACS analysis of HKC8 cells after 24 hours co-culture with PKH26-EVs or vehicle (negative control). **(B)**: Confocal microscopy images of HKC8 after 24 hours co-culture with labeled EVs. Scale bar, 20 μm. Abberivations: BMMSC, bone marrow mesenchymal stem cell; CBMSC, cord blood mesenchymal stem cell; EVs, extracellular vesicles.

into HKC8 cells with a similar efficiency (4,100 ± 1,400 BMMSC-EVs/cell and 4,000 ± 1,500 CBMSC-EVs/cell). The PKH26 signal was preferentially accumulated in the perinuclear area. Intriguingly, incubation of PKH26-stained EVs with parental MSC resulted in dramatically lower incorporation rates than for HKC8 cells (e.g., for BMMSC #1 EVs: Mean Fluorescence Intensity-Ratio, stained versus unstained: HKC8 18.1 ± 4.3, BMMSC #1 2.9 ± 0.7, BMMSC #2 2.1 ± 0.8, CBMSC #1 1.9 ± 0.4, and CBMSC #2 2.3 ± 0.3, $n = 3$). Similar results were obtained with the other combinations of EV and MSC, suggesting a conserved and preferential targeting to non-mesenchymal cells, independently of the MSC type.

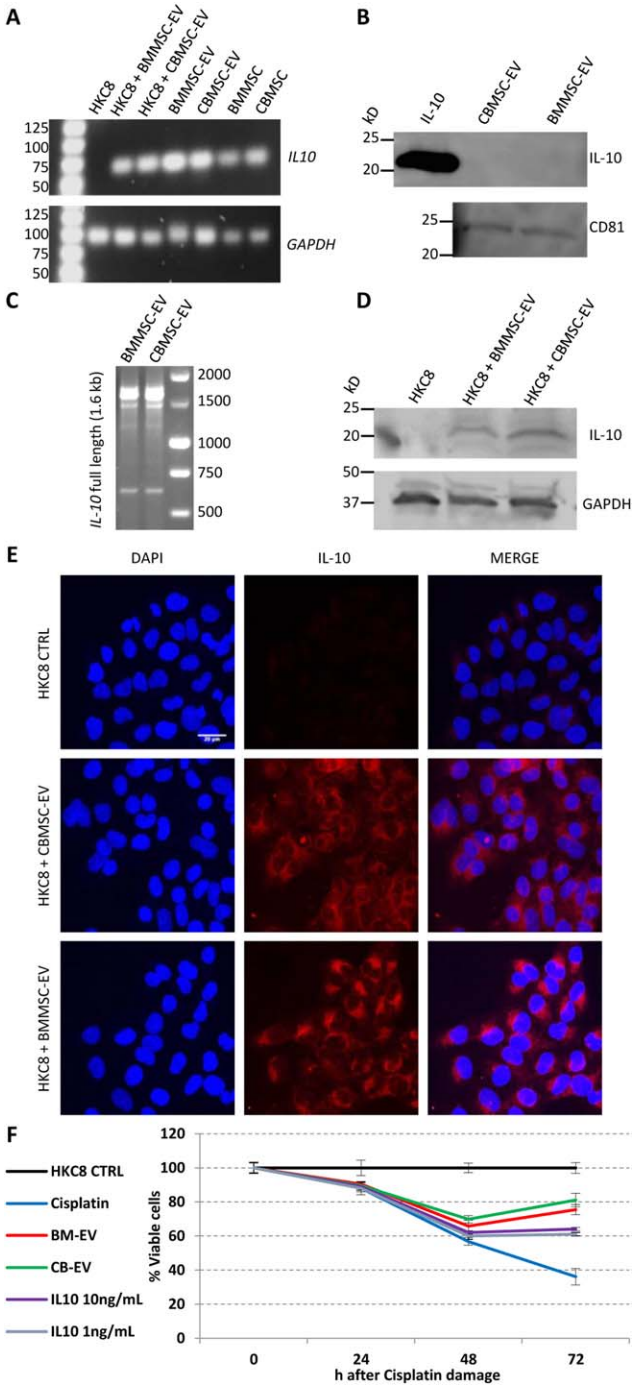

As a proof-of-concept of the anti-inflammatory paracrine activity of MSC-EVs, we chose to track the expression of *IL-10,* which is absent in target HKC8 cells and is present in EVs only as mRNA (Fig. 5A) and not as protein (Fig. 5B). Full-length *IL-10* mRNA was demonstrated to be engulfed in EVs through RT-PCR, being this a prerequisite for efficient translation into a functional protein (Fig. 5C). Then, after EV/HKC8 co-culture, *IL-10* mRNA was identified in HKC8 target cells as confirmation of positive transcript transfer (Fig. 5A). Finally, de novo IL-10 protein expression was detected in tubular HKC8 cells that were co-cultured with either of the MSC-EV type by western blot (Fig. 5D) and immunofluorescence analyses (Fig. 5E). The observed perinuclear localization of IL-10 resembling the ER compartment was due to Brefeldin A treatment to block transport from the ER to the Golgi apparatus to increase the amount of detectable protein (Fig. 5E).

Intriguingly, Soranno and colleagues showed in vivo that delivery of IL-10 following AKI mitigates the local and systemic pro-inflammatory cascade, reducing fibrosis and eventually cell death [33]. Similarly, in vitro IL-10 production after EV administration may resemble such a mechanism and promote viability. Therefore, HKC8 cells where treated with 10 μM cisplatin for 6 hours to mimic acute injury. After drug removal, EVs or recombinant IL-10 were added and cell viability was scored by the MTT assay. Already at 48 hours a protective effect mediated by EVs was observed, which was even further pronounced at 72 hours (Fig. 5F). The recombinant IL-10 control was able to rescue cell viability at lower level. Altogether, these results demonstrate that mRNAs incorporated into MSC-EVs are efficiently transferred to target cells and eventually translated, contributing to the well-known paracrine activities of MSC (Fig. 6).

Discussion

A significant body of literature has shown that the molecular constituents of EVs, especially proteins and microRNAs (miRNA), hold great promise as novel biomarkers for clinical

Figure 5. Incorporation and translation of IL-10 mRNA into HKC8 cells. **(A)**: Agarose gel electrophoresis analysis of *IL-10* mRNA RT-PCR amplification. *GAPDH* mRNA detection is shown as internal control for positive cDNA synthesis. Lane 1, DNA molecular weights. **(B)**: Molecular confirmation of absence of IL-10 protein loading into EVs by Western Blotting analysis. EVs preparations were confirmed for their positivity for the exosomal markers CD81. Purified IL-10 was used as positive control for primary antibody. **(C)**: Agarose gel electrophoresis analysis of *IL-10* intact full-length mRNA (expected 1,589 bp) embedded in MSC-EVs. Lane 3, DNA molecular weights. **(D)**: Western Blot analysis showing absence of IL-10 protein in HKC8 and its appearance after EVs administration. GAPDH was used as positive control for loading. **(E)**: Confocal microscopy images of translated IL-10 protein after MSC-EVs administration to tubular cells. All IL-10 panels show HKC8 cells (with or without EVs supplementation) treated with both primary and secondary antibodies. HKC8 CTRL (not treated with MSC-EVs) confirms endogenous IL-10 absence. Scale bar, 20 μm. **(F)**: MTT test assaying viable cells after cisplatin treatment (Cisplatin) or after drug injury and vesicles or human recombinant IL-10 administration every 24 hours (BM-EVs and CB-EVs). Both vesicles and IL-10 are able to increase recovery and reduce acute injury-driven cell death. Values are related to control cells (HKC8 CTRL) that were not damaged and set as 100% viability for each time point. Abberivations: BMMSC, bone marrow mesenchymal stem cell; CBMSC, cord blood mesenchymal stem cell; EVs, extracellular vesicles.

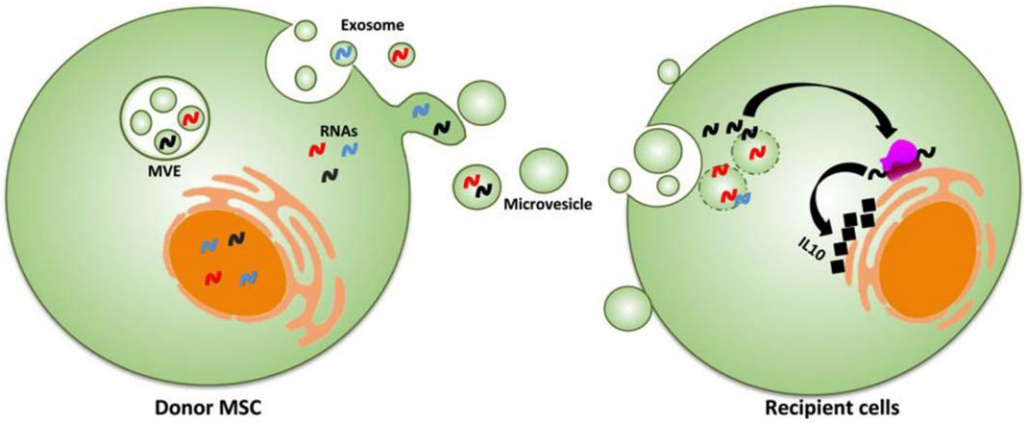

Figure 6. Model of horizontal transfer of EV-embedded mRNA as part of paracrine and autocrine communication network. Abberivations: EVs, extracellular vesicles; MSC, mesenchymal stem cell.

diagnosis [34, 35]. On the contrary, less attention has been devoted to the role of EVs in cell-to-cell communication and fate determination, especially in the stem cell and regenerative medicine fields [36, 37]. A major inadequacy for studying MSC-EVs is that there is no data comparing their clinical efficacy and production feasibility. The majority of studies used only one MSC type, generating controversy on most favorable MSC [13, 14]. A few studies have described efficacy of EVs isolated from different tissues on the same model. For example, bone marrow and Wharton's Jelly MSC were studied for their effects on acute lung injury (ALI) showing similar outcomes [24, 38]. Similarly, BMMSC and umbilical cord-MSC were tested in Liver Injury models [39, 40]. Furthermore, BMMSC- and CBMSC-EVs were shown to protect against ischemic AKI [23, 41]. Despite that the different protocols and experimental settings do not allow for direct comparisons, the similar efficacies observed between these studies suggested conserved properties of MSC-EVs. Our data show, for the first time, that CBMSC and BMMSC are able to secrete vesicles that are almost identical in their physical properties and cargo content, especially for transcripts involved in immunomodulation and proliferation. The only striking difference was the higher EV/cell ratio displayed by CBMSC. This may be relevant for MSC type selection in future clinical applications where it is often desirable to have the highest production rate to minimize cost, space, and time. Furthermore, the kinetics of CBMSC proliferation are substantially higher than those of either adipose derived- or BM-MSC [42, 43]. Therefore, due to their higher proliferation and vesicle secretion rates, CBMSC may be the preferred choice for MSC-EV production.

Despite several reports that MSC-EVs have functions similar to those of MSC, very few of these work have tried to link EV efficacy with the identification of the shuttled active components, mainly proteins [44]. In the context of nucleic acid transfer, main attention has been focused on miRNAs [45]. Very recently, the Camussi group nicely demonstrated the crucial role in miRNA enrichment during EV biogenesis of Alix, an accessory protein of ESCRT, through the interaction with the miRNA binding protein Ago2 [46]. Similarly, EV enrichment of other extracellular RNAs, including mRNAs, may depend on their association with specific subsets of RNA-binding proteins. Intriguingly, EVs released from the human liver stem-like cells were shown to contain members of several families of RNA-binding proteins, each specific for a different transcript motif [29]. Consistent with this hypothesis, Bruno and coworkers suggested that BMMSC-EVs may also engulf a specific subset of mRNAs rather than a random sample of cellular mRNA [23].

In this study, we identified a subgroup of mRNAs that are preferentially loaded into MSC-EVs, thus potentiating their role in intercellular communication. *FGF7*, which is expressed at very low levels in donor CBMSC, was among most enriched transcripts in both types of MSC-EVs, suggesting a pivotal function. Supporting this notion, Zhu and coworkers demonstrated that BMMSC-EVs were therapeutically effective following *E. coli* endotoxin-induced ALI in mice through the expression of EV-transferred *FGF7* mRNA in the injured alveolus [24]. Therefore, FGF7 protein expression from MSC-EV mRNA restored lung protein permeability and reduced alveolar inflammation, although through a still unknown mechanism. Similar functions may be postulated for *IL-10* mRNA, which we demonstrated to be highly enriched in EVs and efficiently translated in kidney tubular cells. We have demonstrated previously that MSC supernatant administration in mice with cisplatin-induced AKI ameliorated both renal function and tubular cell injury, and prolonged survival [32]. Moreover, MSC-EVs treatment after kidney injury prevents renal fibrosis [23]. These effects were intriguingly similar to those observed upon IL-10 administration [33], that in the adult kidney is secreted by mesangial cells [47]. Thus, due to absence of IL-10 protein in MSC-EVs, *IL-10* mRNA transfer and translation may be a novel mechanism of the complex recovery and anti-inflammatory processes recently proposed for in vivo kidney repair by MSC [48]. In fact, existence of such new paradigm in tubular cells has been confirmed by the in vitro MSC-EV mediated transfer of *IGF-1R* mRNA that, after translation, potentiates tubular cell sensitivity to locally produced IGF-1 [49]. Similarly, translated IL-10 may enhance IL-10/IL-10R1R2 anti-inflammatory pathway at tubular cell level, suggesting a potential therapeutic role for *IL-10* mRNA transfer from EVs. Altogether, these data provide a new mechanism to explain how the restricted homing of MSC at the site of injury may still result in enhanced protective effects via gene-based communication amplified through the enrichment of therapeutic mRNAs in EVs.

In addition to the transfer of therapeutic mRNAs, the enrichment of mRNAs with specific 3′UTR sequences into EVs may also have a role in modulating target cells, as was

reported in glioblastoma-EVs [30]. One intriguing possibility is that miRNA binding sites in 3′UTRs, may compete with target cell RNAs for binding in order to alter mRNA stability and translation. Our in silico analysis showed that the 3′UTR of preferentially enriched mRNAs may interact with at least 73 different miRNAs, potentially affecting the stability and thus translation of more than 2,000 transcripts. Intriguingly, the top biological processes altered by their products were related to RNA transcription and metabolism, gene expression and anti-apoptotic processes. These categories are strictly related, because increase in RNA synthesis and translation have potent inhibitory effects on apoptotic processes [50]. Consistently, MSC-EV administration resulted in strong anti-apoptotic and pro-proliferative outcomes in both in vitro [23, 51, 52] and in vivo experimental models [40, 53]. Thus, transcripts incorporated into MSC-EVs may regulate target cells to different levels, increasing the array of targets addressed by vesicles and shuttled factors.

Conclusion

In summary, we demonstrated that MSC load specific transcripts into secreted EVs independently of their cytosolic abundance, suggesting purposeful transfer to target cells. These transferred molecules may act directly through their protein products or interact with other nucleic acids or nucleic acid-binding proteins. These results shed new light on the knowledge of a complex and still uncharacterized mechanism involving EVs as factors of MSC autocrine and paracrine action.

Acknowledgments

This study has been in part supported by "Ricerca Corrente Fondazione IRCCS Ca' Granda Ospedale Maggiore Policlinico Milano" 2015 and Italian program of liberal donation for research "5 per mille" 2015 (to Lorenza Lazzari). Authors thank Dr. Marianna Di Francesco for her valuable help with SEM data acquisition and interpretation. This work was part of the Ph.D. project of Mario Barilani for the Ph.D. School in Biosciences and Biotechnology curriculum Cell Biology of the University of Padoa.

Author Contributions

E.R.: conception and design, collection and assembly of data, data analysis and interpretation, manuscript writing, final approval of manuscript; F.B.: conception and design, collection and assembly of data, data analysis and interpretation, final approval of manuscript; M.B., V.P., A.C., P.L., V.D., and V.B.: collection and assembly of data, final approval of manuscript; L.L.: conception and design, final approval of manuscript.

Disclosure of Potential Conflicts of Interest

The authors indicate no potential conflicts of interest.

References

1 Ullah I, Subbarao RB, Rho GJ. Human mesenchymal stem cells - Current trends and future prospective. Biosci Rep 2015;35:e00191.
2 Crisan M, Corselli M, Chen CW et al. Multilineage stem cells in the adult: A perivascular legacy?. Organogenesis 2011;7:101–104.
3 Stoltz JF, de Isla N, Li YP et al. Stem cells and regenerative medicine: Myth or reality of the 21th century. Stem Cells Int 2015;2015:734731.
4 Gao F, Chiu SM, Motan DA et al. Mesenchymal stem cells and immunomodulation: Current status and future prospects. Cell Death Dis 2016;7:e2062.
5 Najar M, Raicevic G, Fayyad-Kazan H et al. Mesenchymal stromal cells and immunomodulation: A gathering of regulatory immune cells. Cytotherapy 2016;18:160–171.
6 Ferrand J, Noel D, Lehours P et al. Human bone marrow-derived stem cells acquire epithelial characteristics through fusion with gastrointestinal epithelial cells. PLoS One 2011;6:e19569.
7 Spees JL, Olson SD, Ylostalo J et al. Differentiation, cell fusion, and nuclear fusion during ex vivo repair of epithelium by human adult stem cells from bone marrow stroma. Proc Natl Acad Sci USA 2003;100:2397–2402.
8 Vassilopoulos G, Wang PR, Russell DW. Transplanted bone marrow regenerates liver by cell fusion. Nature 2003;422:901–904.
9 Ringdén O, Uzunel M, Rasmusson I et al. Mesenchymal stem cells for treatment of therapy-resistant graft-versus-host disease. Transplantation 2006;81:1390–1397.
10 Lee RH, Pulin AA, Seo MJ et al. Intravenous hMSC improve myocardial infarction in mice because cells embolized in lung are activated to secrete the anti-inflammatory protein TSG-6. Cell Stem Cell 2009;5:54–63.
11 Parekkadan B, Milwid JM. Mesenchymal stem cells as therapeutics. Annu Rev Biomed Eng 2010;12:87–117.
12 Yáñez-Mó M, Siljander PR, Andreu Z et al. Biological properties of extracellular vesicles and their physiological functions. J Extracell Vesicles 2015;4:27066.
13 Rani S, Ryan AE, Griffin MD et al. Mesenchymal stem cell-derived extracellular vesicles: Toward cell-free therapeutic applications. Mol Ther 2015;5:812–823.
14 Yu B, Zhang X, Li X. Exosomes derived from mesenchymal stem cells. Int J Mol Sci 2014;15:4142–4157.
15 Ragni E, Lommel M, Moro M et al. Protein O-mannosylation is crucial for human mesencyhmal stem cells fate. Cell Mol Life Sci 2016;73:445–458.
16 Dominici M, Le Blanc K, Mueller I et al. Minimal criteria for defining multipotent mesenchymal stromal cells. The International Society for Cellular Therapy position statement. Cytotherapy 2006;8:315–317.
17 Ragni E, Viganò M, Rebulla P et al. What is beyond a qRT-PCR study on mesenchymal stem cell differentiation properties: How to choose the most reliable housekeeping genes. J Cell Mol Med 2013;17:168–180.
18 Deng J, Kohda Y, Chiao H et al. Interleukin-10 inhibits ischemic and cisplatin-induced acute renal injury. Kidney Int 2001;60:2118–2128.
19 Mu W, Ouyang X, Agarwal A et al. IL-10 suppresses chemokines, inflammation, and fibrosis in a model of chronic renal disease. J Am Soc Nephrol 2005;16:3651–3660.
20 Deregibus MC, Cantaluppi V, Calogero R et al. Endothelial progenitor cell-derived microvesicles activate an angiogenic program in endothelial cells by a horizontal transfer of mRNA. Blood 2007;110:2440–2448.
21 Valadi H, Ekström K, Bossios A et al. Exosome-mediated transfer of mRNAs and microRNAs is a novel mechanism of genetic exchange between cells. Nat Cell Biol 2007;9:654–659.
22 Bolstad BM, Irizarry RA, Astrand M et al. A comparison of normalization methods for high density oligonucleotide array data based on variance and bias. Bioinformatics 2003;19:185–193.
23 Bruno S, Grange C, Deregibus MC et al. Mesenchymal stem cell-derived microvesicles protect against acute tubular injury. J Am Soc Nephrol 2009;20:1053–1067.
24 Zhu YG, Feng XM, Abbott J et al. Human mesenchymal stem cell microvesicles for treatment of Escherichia coli endotoxin-induced acute lung injury in mice. Stem Cells 2014;32:116–125.
25 Vandesompele JD, Preter K, Pattyn F et al. Accurate normalization of real-time quantitative RT-PCR data by geometric averaging of multiple internal control genes. Genome Biol 2002;3:RESEARCH0034.
26 D'haene B, Mestdagh P, Hellemans J et al. miRNA expression profiling: From reference genes to global mean normalization. Methods Mol Biol 2012;822:261–272.

27 Bolukbasi MF, Mizrak A, Ozdener GB et al. miR-1289 and "zipcode"-like sequence enrich mRNAs in microvesicles. Mol Ther Nucleic Acids 2012;1:e10.
28 Batagov AO, Kuznetsov VA, Kurochkin IV. Identification of nucleotide patterns enriched in secreted RNAs as putative cis-acting elements targeting them to exosome nanovesicles. BMC Genomics 2011;12:S18.
29 Waris S, Wilce MC, Wilce JA. RNA recognition and stress granule formation by TIA proteins. Int J Mol Sci 2014;15:23377–23388.
30 Batagov AO, Kurochkin IV. Exosomes secreted by human cells transport largely mRNA fragments that are enriched in the 3'-untranslated regions. Biol Direct 2013;8:12.
31 Dweep H, Gretz N, Felekkis K. A schematic workflow for collecting information about the interaction between copy number variants and microRNAs using existing resources. Methods Mol Biol 2014;1182:307–320.
32 Morigi M, Rota C, Montemurro T et al. Life-sparing effect of human cord blood-mesenchymal stem cells in experimental acute kidney injury. Stem Cells 2010;28:513–522.
33 Soranno DE, Rodell CB, Altmann C et al. Delivery of interleukin-10 via injectable hydrogels improves renal outcomes and reduces systemic inflammation following ischemic acute kidney injury in mice. Am J Physiol Renal Physiol 2016;311:F362–F372.
34 Liu Y, Lu Q. Extracellular vesicle microRNAs: Biomarker discovery in various diseases based on RT-qPCR. Biomark Med 2015;9:791–805.
35 Fujita Y, Yoshioka Y, Ochiya T. Extracellular vesicle transfer of cancer pathogenic components. Cancer Sci 2016;107:385–390.
36 Quesenberry PJ, Aliotta J, Deregibus MC et al. Role of extracellular RNA-carrying vesicles in cell differentiation and reprogramming. Stem Cell Res Ther 2015;6:153.
37 Nawaz M, Fatima F, Vallabhaneni KC et al. Extracellular vesicles: Evolving factors in stem cell biology. Stem Cells Int 2016;2016:1073140.
38 Lee C, Mitsialis SA, Aslam M et al. Exosomes mediate the cytoprotective action of mesenchymal stromal cells on hypoxia-induced pulmonary hypertension. Circulation 2012;126:2601.
39 Li T, Yan Y, Wang B et al. Exosomes derived from human umbilical cord mesenchymal stem cells alleviate liver fibrosis. Stem Cells Dev 2013;22:845–854.
40 Tan CY, Lai RC, Wong W. Mesenchymal stem cell-derived exosomes promote hepatic regeneration in drug-induced liver injury models. Stem Cell Res Ther 2014;5:76.
41 Kilpinen L, Impola U, Sankkila L et al. Extracellular membrane vesicles from umbilical cord blood-derived MSC protect against ischemic acute kidney injury, a feature that is lost after inflammatory conditioning. J Extracell Vesicles 2013;2:21927.
42 Zhang X, Hirai M, Cantero S et al. Isolation and characterization of mesenchymal stem cells from human umbilical cord blood: Reevaluation of critical factors for successful isolation and high ability to proliferate and differentiate to chondrocytes as compared to mesenchymal stem cells from bone marrow and adipose tissue. J Cell Biochem 2011;112:1206–1218.
43 Barilani M, Lavazza C, Viganò M et al. Dissection of the cord blood stromal component reveals predictive parameters for culture outcome. Stem Cells Dev 2015;24:104–114.
44 Shentu TP, Wong S, Espinoza C et al. Extracellular vesicles isolated from human mesenchymal stem cells promote resolution of pulmonary fibrosis. FASEB J 2016;30 no. 1 Supplement 160.2.
45 Chen TS, Lai RC, Lee MM et al. Mesenchymal stem cell secretes microparticles enriched in pre-microRNAs. Nucleic Acids Res 2010;1:215–224.
46 Iavello A, Frech VS, Gai C et al. Role of Alix in miRNA packaging during extracellular vesicle biogenesis. Int J Mol Med 2016;37:958–966.
47 Jin Y, Liu R, Xie J et al. Interleukin-10 deficiency aggravates kidney inflammation and fibrosis in the unilateral ureteral obstruction mouse model. Lab Invest 2013;93:801–811.
48 Morigi M, Benigni A. Mesenchymal stem cells and kidney repair. Nephrol Dial Transplant 2013;28:788–793.
49 Tomasoni S, Longaretti L, Rota C et al. Transfer of growth factor receptor mRNA via exosomes unravels the regenerative effect of mesenchymal stem cells. Stem Cells Dev 2013;22:772–780.
50 Bushell M, Stoneley M, Sarnow P et al. Translation inhibition during the induction of apoptosis: RNA or protein degradation?. Biochem Soc Trans 2004;32:606–610.
51 Bruno S, Grange C, Collino F et al. Microvesicles derived from mesenchymal stem cells enhance survival in a lethal model of acute kidney injury. PLoS One 2012;7:e33115.
52 Zhang B, Wang M, Gong A et al. HucMSC-exosome mediated-Wnt4 signaling is required for cutaneous wound healing. Stem Cells 2015;33:2158–2168.
53 Gatti S, Bruno S, Deregibus MC et al. Microvesicles derived from human adult mesenchymal stem cells protect against ischaemia-reperfusion-induced acute and chronic kidney injury. Nephrol Dial Transplant 2011;26:1474–1483.
54 Carmona-Saez P, Chagoyen M, Tirado F et al. GENECODIS: A web-based tool for finding significant concurrent annotations in gene lists. Genome Biol 2007;8:R3.
55 Deans RJ, Moseley AB. Mesenchymal stem cells. Exp Hematol 2000;28:875–884.
56 Nogales-Cadenas R, Carmona-Saez P, Vazquez M et al. GeneCodis: Interpreting gene lists through enrichment analysis and integration of diverse biological information. Nucleic Acids Res 2009;37:W317–W322.
57 Tabas-Madrid D, Nogales-Cadenas R, Pascual-Montano A. GeneCodis3: A non-redundant and modular enrichment analysis tool for functional genomics. Nucleic Acids Res 2012;40:W478–W483.


See www.StemCellsTM.com for supporting information available online.